J. Microbiol. Biotechnol. (2019), 29(6), 897–904
https://doi.org/10.4014/jmb.1902.02036

jmb

Polyaromatic Resin HP-20 Induced Accumulation of Intermediate Azaphilones in *Monascus purpureus* Δ*mppC* and Δ*mpp7* Strains S

Yoon Ji Lim[1], Doh Won Lee[1], Jeong Ju Choi[1], Si-Hyung Park[2], and Hyung-Jin Kwon[1]*

[1]*Department of Biological Sciences and Bioinformatics, Myongji University, Yongin 17058, Republic of Korea*
[2]*Department of Oriental Medicine Resources and Institute for Traditional Korean Medicine Industry, Mokpo National University, Muan-gun, Jeollanam-do, 58554, Republic of Korea*

Received: February 22, 2019
Revised: May 12, 2019
Accepted: May 13, 2019

First published online
May 14, 2019

**Corresponding author*
Phone: +82-31-330-6470;
Fax: +82-31-335-7248;
E-mail: hjink@mju.ac.kr

Supplementary data for this paper are available on-line only at http://jmb.or.kr.

pISSN 1017-7825, eISSN 1738-8872

Monascus purpureus recombinant *mppC* and *mpp7* knockout strains were subjected to extractive fermentation in the context of azaphilone pigment production. Inclusion of Diaion HP-20 resin resulted in the selective production of unreduced azaphilone congeners, in addition to the early intermediate FK17-P2a, from Δ*mppC* and Δ*mpp7* strains that would otherwise mainly produce reduced congeners. Structural determination of two novel unreduced azaphilones from the Δ*mpp7* strain was accomplished. The unreduced azaphilone compound was converted into the cognate reduced congener in recombinant *M. purpureus* strains, demonstrating its intermediate role in azaphilone biosynthesis. This study demonstrates the possibility that extractive fermentation with Diaion HP-20 resin can be used to obtain cryptic azaphilone metabolites.

Keywords: Azaphilone, extractive fermentation, HP-20 resin, intermediate, *Monascus purpureus*

Introduction

Monascus species, including *M. anka*, *M. pilosus*, *M. purpureus* and *M. ruber*, are filamentous fungi that have been widely used for food fermentation in East Asia [1]. *Monascus* species are highly productive of pigments that belong to an azaphilone (Az) class of polyketides [2–4]. With this property, *Monascus* has been used as the source of a food colorant [5]. The major members of *Monascus* Azs (MAzs) are monascin (**1**), ankaflavin (**2**), rubropunctatin (**3**), monascorubrin (**4**), rubropunctamine (**5**), and monascorubramine (**6**) (Fig. 1). Although MAz is widely known as a natural food colorant, the health benefits of MAz components were also substantiated; anti-atherosclerosis [6], anti-diabetic [7], anti-inflammatory [8], and anti-obesity [9] activity are significant for the yellow components (**1** and **2**). The *Monascus* extract enriched with **1** and **2** (ANKASCIN 568-R) was marketed as a dietary supplement and its disease-alleviating activities, including the regulation of blood sugar and lipid level, were documented [10–12]. Anti-cancer potential of **3** was also reported [13–15].

MAz is produced by the catalysts encoded in the MAz biosynthetic gene cluster (BGC) that harbors *MpPKS5*, the gene encoding a non-reducing polyketide synthase (PKS) with a reductive release domain [16]. MAz biosynthesis is postulated to operate through FK17-P2a, which is produced by MpPKS5 with the assistance of a reductase MppA and a hydrolase MppD [17, 18] (Fig. 1). It is proposed that FK17-P2a is converted to azanigerone E by a hydroxylase MppF. The intermediate role of FK17-P2a and azanigrone E was first characterized in azanigerone pathway of *Aspergillus niger* [19] and was then substantiated in MAz biosynthesis [17, 20]. Azanigerone E was identified in the gene inactivation mutants of *Mpfas2* and *mppB* orthologue (*mrpigJK* and *mrpigD*, respectively) in *M. ruber* [20]. The 3-oxo-octanoyl or -decanoyl moiety that is synthesized by a canonical fatty acid synthase (MpFAS2) encoded in MAz BGC is proposed to be added to azanigerone E by MppB acyltransferase [20, 21]. The following biochemical modifications were also characterized in MAz biosynthesis [17, 22]. In details,

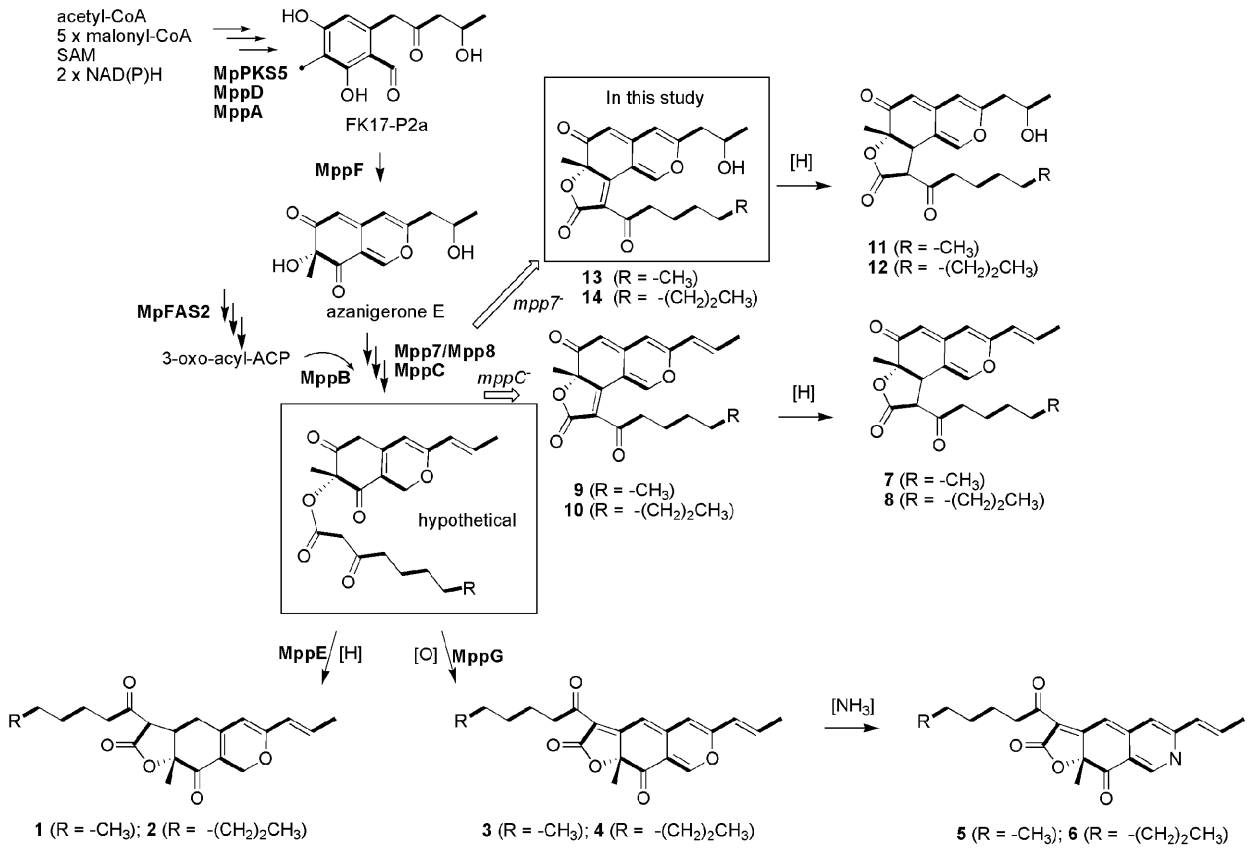

Fig. 1. Structures of MAz compounds with their proposed biosynthetic pathway.
To emphasize their biosynthetic origins, the acetate units are denoted with bars and the *S*-adenosyl-L-methionine-derived methyl carbon is indicated with a black dot in FK17-P2a.

M. purpureus Δ*mppC* strain produced **7** to **10** [17]. Knoevenagel condensation between azanigerone E and 3-oxo-acyl moieties is proposed to generate **9** and **10,** which are hypothesized to be reduced to **7** and **8**, respectively (Fig. 1). Inactivation of *mpp7* gene resulted in the production of **11** and **12**, suggesting the dehydratase role of Mpp7 [22]. The *O*-acetylase activity of MrPigM (Mpp7) and deacetylase role of MrPigO (Mpp8) in the dehydration were later characterized in MAz biosynthesis of *M. ruber* [20]. The Knoevenagel condensation scenario predicted that the production of **11** and **12** resulted from the reduction of **13** and **14**, both of which, however, were not identified.

Final oxidative and reductive modifications form a divergent pathway for reduced (yellow; **1** and **2**) and oxidized (orange; **3** and **4**) congeners, respectively [23, 24]. Primary amine derivatives non-enzymatically convert **3** and **4** into their cognate versions of **5** and **6**, respectively [4, 16]. The name azaphilone is derived from this azaphilic character, the tendency to aminate, while **1** and **2** are actually not azaphilic at all, though they are routinely included in the Az group.

Extractive fermentation (EF) is a general term for any fermentation method with simultaneous product extraction. It is generally accepted that EF minimizes product inhibition inside cells to promote the product yield. EF can be achieved simply by enhancing the capacity of the culture supernatant (SN) to accommodate the product. EF of a *Monascus anka* strain with the nonionic detergent Triton X-100 (TX100) was found to promote the export of MAzs [25–28]. It was recently demonstrated that the production of oxidized (orange) MAz congeners **3** and **4** was promoted in the EF of *M. purpureus* [29]. This study demonstrated that the polyaromatic absorbent resin Diaion HP-20 (HP20) induced the accumulation of FK17-P2a, which highlights the possibility that HP20-EF induces the accumulation of intermediate compounds in MAz biosynthesis. This study also shows that HP20-EF is capable of inducing accumulation of FK17-P2a and unreduced Az derivatives, the biological intermediates of the reduced ones, in both Δ*mppC* and Δ*mpp7* strain.

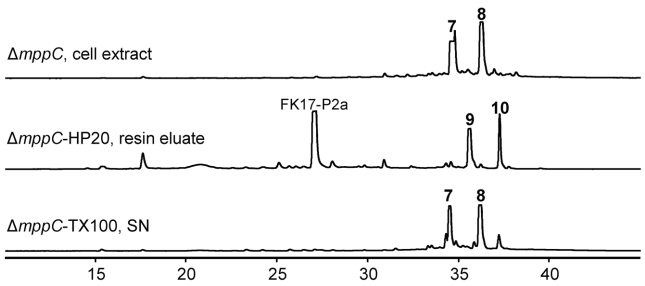

Fig. 2. Accumulation of **9**, **10**, and FK17-P2a in HP20-EF of the Δ*mppC* strain.

HPLC traces, monitored at 330 nm and drawn to the same Y-scale, are shown for the control-cell methanol extract, HP20-EF-resin methanol eluate, and TX100-EF-SN diethyl ether extract. Azs **7** to **10** are indicated with their numerical annotations, and FK17-P2a is also indicated.

Materials and Methods

Culture Conditions

Monascus purpureus KACC 42430 (DSM 1379) was used in this study. *M. purpureus* recombinant strains were cultured on potato dextrose agar (PDA) at 30°C for 7 days. Agar blocks retrieved from the PDA culture were used to inoculate potato dextrose broth (PDB; Gellix, Ventech Bio, Korea). The liquid submerged cultures, prepared in a 50 ml culture volume in a 250 ml baffled flask, were maintained in a rotary shaker at 30°C for 7 days with a shaking speed of 250 rpm. Ten milliliters of Diaion HP-20 resin (HP20; Samyang Co., Korea) or 2.5 ml of Triton X-100 (TX100; Amresco, USA) was added to the PDB media at the initiation of the culture in EF.

From the submerged culture, mycelia were separated from the supernatant (SN) by passing through a filter paper under reduced pressure. HP20 was collected together with mycelia in HP20-EF sample and HP20 was separated from mycelia by passing through a disposable net strainer (approximately 1 mm pore). By repeatedly applying water flow with a wash bottle, we made a majority of HP20 pass through the net strainer. We assumed that no less than 90% HP20 was recovered this way. For the compound isolation from HP20-EF of the Δ*mpp7* strain, the collected mycelia and HP20 were processed without separating the resin for convenience. The mycelia and HP20 were then extracted with methanol of the culture volume. Diethyl ether was the solvent to extract SN. The extract was evaporated under a reduced pressure and the residue was dissolved in methanol for chemical analyses.

For the bioconversion experiment, 50 ml PDB cultures of the *M. puprureus* recombinant strains were maintained for 3 days before dispensing 5 ml in 50 ml culture tubes. In the Δ*MpPKS5* experiment, 400 µl methanol solutions of **13** at 2.5, 5, and 10 mM were added to make the final concentrations of 0.2, 0.4, and 0.8 mM, respectively. For other recombinant strains, 0.3 mM **13** (150 µl of 10 mM **13** to 5 ml) was applied. The control sample was added with the same amount of methanol as the **13** solution. These tubes were incubated in a rotary shaker at 30°C for 1 day with a shaking speed of 200 rpm before extraction for analysis. The mycelia and SN were extracted with methanol and chloroform, respectively. The extract was evaporated under a reduced pressure and the residue was dissolved in methanol for chemical analyses.

Chemical Analysis and Chromatography Methods

Thin-layer chromatography (TLC) was performed on silica gel 60 F_{254} TLC plates (Merck, Germany), which were developed with n-hexane/ethyl acetate/formic acid (24:18:1, by vol.). The isolation of MAz compounds from HP20-EF of the Δ*mpp7* strain was achieved through chromatographic separation on an HP20, ODS-A gel (particle size of 75 µm, pore size of 12 nm; YMC, USA), and a silica gel 60 (0.040–0.063 mm; Merck). HP20 and ODS-A gel chromatography were developed with water to methanol, and the silica gel 60 column was eluted with n-hexane to ethylacetate. The eluate fractions were examined by TLC.

Ultraviolet (UV)-visible absorption spectra were collected with a Cary50 spectrophotometer (Varian, USA). For the culture experiments, the absorption spectra were collected with proper dilutions in methanol, and the values were converted to the corresponding values in the original culture volume. In measuring UV-visible absorption, the SN was directly applied without extraction while the methanolic extract was used for the cell or HP20 absorption measurement.

High-performance liquid chromatography (HPLC) analysis was performed on a Prostar system (Varian) with a Gemini C18 column (150 × 3.0 mm, particle size of 5 µm, pore size of 11 nm; Phenomenex, USA) and the elution was monitored at 330 nm. The mobile phase consisted of 0.1% formic acid in water (A) and 0.1% formic acid in acetonitrile (B). The flow rate was maintained at 0.5 ml/min. The system was run with the following gradient program: 100% A for 5 min, from 100% A to 70% A over 20 min, from 70% A to 100% B over 10 min, then maintained at 100% B for 10 min.

LC-mass spectrometry (MS) analysis was performed with a Dionex UltiMate 3000 UHPLC (Thermo Scientific, USA) combined with a LTQ XL Orbitrap mass spectrometer (Thermo Scientific, Germany) on a reverse-phase Kinetex column (100 mm × 2.1 mm, particle size of 1.7 µm, pore size of 10 nm; Phenomenex), which was maintained at 40°C. The flow rate was maintained at 0.2 ml/min. Gradient elution was performed with the mobile phase composed of 0.1% formic acid in water (A) and 0.1% formic acid in acetonitrile (B). The LC gradient elution was applied with the following program: from 90% A to 50% A over 20 min, from 50% A to 100% B over 10 min, then maintained at 100% B for 10 min. Electrospray ionization (ESI) was performed in positive-ion mode and mass spectra were obtained in Fourier-transform mode with resolution of R = 30,000 at *m/z* 400. Metabolites were detected by full-scan mass analysis from *m/z* 200 to 500.

High-resolution mass analysis of **13** and **14** was conducted in fast atom bombardment (FAB) ionization method using a JMS-70

mass spectrometer (JEOL, Japan). Optical rotations were recorded in 0.1% (w/v) methanol solution on a JASCO P-2000 digital polarimeter (JASCO, Japan). The nuclear magnetic resonance (NMR) experiments such as ^{1}H NMR, ^{13}C NMR, ^{1}H–^{1}H correlation spectroscopy, ^{1}H–^{13}C heteronuclear single quantum coherence (HSQC), and ^{1}H–^{13}C heteronuclear multiple bond correlation (HMBC), were conducted in pure $CDCl_3$ at 23°C using a 400 MHz Varian MR-400 spectrometer.

Results and Discussion

HP20-EF Promoted Accumulation of Unreduced Azs and FK17-P2a in the Δ*mppC* Strain

The *M. purpureus* Δ*mppC* strain lacks MppC reductase activity and produces **7** to **10** instead of the major MAzs **1** to **4** pigment [17] (Fig. 1). Azs **7** and **8** are the main products of the Δ*mppC* strain in a PDB batch culture. It was also reported that the levels of **9** and **10** were limited in the cognate recombinant strain of *Monascus ruber* [20]. This situation was the motivation of this EF study, urging us to pursue a culture condition affording **9** and **10**. EF of the Δ*mppC* strain with TX100 or HP20 promoted the export of the pigment Az as found with ultraviolet (UV)-visible absorption analysis (Fig. S1). The absorption profile of the SN from the TX100-EF was comparable to the methanolic cell extract of the control culture, while the pattern of the methanol eluate of the HP20 resin from the HP20-EF was clearly distinguishable from both of them, with a dramatic reduction in absorbance at around 380 nm. HPLC analysis indicated that the peaks of **7** and **8** were replaced with those of **9** and **10** in the HP20 methanol eluate of HP20-EF (Fig. 2). HP20-EF also accumulated FK17-P2a, the early intermediate of MAz biosynthesis. Azanigerone E, the other biosynthetic intermediate, was not found in HP20-EF, however. Notably, TX100 was incapable of causing this profile shift.

Liquid chromatography-mass spectrometry (LC-MS) analysis confirmed the induction of FK17-P2a, **9** and **10** in HP20-EF (Figs. S2 and S3). Positive ESI mass analysis supported the identities of **7** to **10** by the detection of 357.169, 385.200, 355.154, and 383.184 *m/z* signals, respectively, for $[M+H]^+$ ions, where the calculated exact masses are 357.170 ($C_{21}H_{25}O_5^+$), 385.201 ($C_{23}H_{29}O_5^+$), 355.154 ($C_{21}H_{23}O_5^+$), and 383.185 ($C_{23}H_{27}O_5^+$), respectively (Fig. S2). The UV-visible absorption spectra, collected in the LC elution, of the reduced Az compounds (**9** and **10**) were distinguishable from the unreduced congeners (**7** and **8**) (Fig. 2), with a broad absorption peak at 380 nm for the former and at 355 nm for the latter. This absorption pattern was consistent with the UV-visible absorption spectra of the crude samples (Fig. S1). The peak of FK17-P2a displayed a 253.107 *m/z* signal for $[M+H]^+$ ions, where the calculated exact masses are 253.107 ($C_{13}H_{17}O_5^+$), and the UV-visible absorption peak was found at 295 nm (Fig. S3). Azs **7** and **8** mainly accumulated inside the cells of the Δ*mppC* strain and supplementation with HP20 gave rise to the accumulation of **9** and **10**, in addition to FK17-P2a, by promoting their export. Because **9** and **10** are the proposed precursors of **7** and **8**, respectively, it could be suggested that HP20-EF induced accumulation of intermediate Azs in the Δ*mppC* strain.

HP20-EF Induced Accumulation of Unreduced Azs and FK17-P2a in the Δ*mpp7* Strain

The Δ*mpp7* strain was generated by abolishing the Mpp7-involved dehydration step and was found to produce **11** and **12** instead of the major MAz **1** to **4** pigments [22] (Fig. 1). The biosynthesis of **11** and **12** was proposed to involve **13** and 14 [22]. This implied that **13** and **14** serve as intermediates to **11** and **12**, respectively, but the former compounds were not found in the Δ*mpp7* strain before this study. Consistently, the cognate recombinant strain of *Monascus ruber* did not produce **13** and **14** [20]. In this study, the Δ*mpp7* strain was applied to HP20-EF to afford the production of **13** and **14**. Unlike the Azs from the wild-type *M. purpureus* and Δ*mppC* strain, a significant portion of **11** and **12** was exported into the SN [22], which was also found in this study (Fig. S4). Both the cell extract and SN of the Δ*mpp7* strain culture displayed an absorption peak at 360 nm. Similar to the case of the Δ*mppC* strain, the pigment was mainly found in the methanol eluate of the resin in HP20-EF of the Δ*mpp7* strain, and its UV-visible absorption peak was found at 340 nm, shifted to a lower wavelength compared to that of the control (Fig. S4). HPLC analysis demonstrated that HP20 induced the accumulation of FK17-P2a and two new metabolites, which were tentatively assigned as **13** and **14**, while suppressing the production of **11** and **12** in the Δ*mpp7* strain (Fig. 3). LC-MS analysis supported the identities of **13** and **14** as the unreduced congener by the detection of 373.164 and 401.196 *m/z* signals, respectively, for $[M+H]^+$ ions, where the calculated exact masses are 373.164 ($C_{21}H_{25}O_6^+$) and 401.196 ($C_{23}H_{29}O_6^+$), respectively (Fig. S5). The peaks of **11** and **12** displayed 375.180 and 403.211 signals, respectively, for $[M+H]^+$ ions, where the calculated exact masses are 375.180 ($C_{21}H_{27}O_6^+$) and 403.211 ($C_{23}H_{31}O_6^+$), respectively. Azs **11** and **12** displayed UV-visible absorption peaks at 360 nm, while **13** and **14** displayed peaks at 267 and 344 nm. This observation supports that HP20-EF is capable

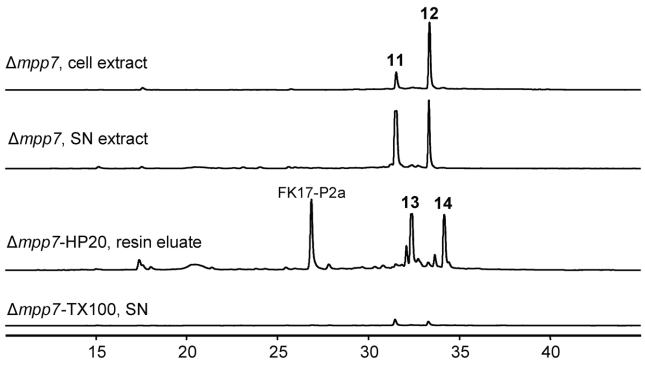

Fig. 3. Accumulation of **13**, **14**, and FK17-P2a in HP20-EF of the Δ*mpp7* strain.

HPLC traces, monitored at 330 nm and drawn to the same Y-scale, are shown for the control-cell methanol extract, control-SN diethyl ether extract, HP20-EF-resin methanol eluate, and TX100-EF-SN diethyl ether extract. Azs **11** to **14** are indicated with their numerical annotations, and FK17-P2a is also indicated.

of inducing the accumulation of unreduced (intermediate) Az congeners by exporting them in the Δ*mpp7* strain and provides an example of uncovering cryptic Az compounds with HP20-EF.

Notably, the production of Az compounds is limited in TX100-EF, and there is no evidence for **13** and **14** (Figs. 3 and S6). As observed in TX100-EF of the Δ*mppC* strain, a strong ion peak of TX100 was found at 27 min in the LC-MS analysis (Fig. S6). This peak showed an absorption peak at 277 nm and a mass pattern with an increment of *m/z* 44.026 (C_2H_4O), which is in agreement with the chemical composition of TX100 ingredients. Note that the *m/z* detection range of this mass analysis was set below 500, which did not allow the detection of the main ingredients of TX100.

Isolation and Structural Determination of 13 and 14

Before conducting a culture (500 ml) for isolation of **13** and **14**, we checked whether a liquid culture-inoculation is as effective as the agar culture-inoculation in producing **13** and **14** in HP20-EF. The HP20-EF PDB culture of the Δ*mpp7* strain was established with 10% (v/v) inoculation of the PDB liquid culture, and a high agitation culture (250 rpm) was compared with a low speed agitation culture (100 rpm). It was previously reported that the agitation speed affects the MAz production profile, the relative composition of reduced (**1** and **2**) and oxygenated (**3** and **4**) congeners [29]. The low agitation culture was found to promote the production of **1** and **2**, while suppressing that of **3** and **4**, in *M. purpureus*. Induction of **13** and **14** was evident in the high agitation culture but the yield was relatively low (Fig. S7A). In the low agitation culture, the productivity of **11** and **12** was maintained and **13** and **14** were found as minor components (Fig. S7B). These results indicated that the liquid culture-inoculation was not as effective as the agar culture-inoculation in producing **13** and **14** in HP20-EF and guided us to prepare ten flasks of 50 ml HP20-EF culture with the agar blocks of the Δ*mpp7* PDA culture.

Azs **13** and **14** were isolated through chromatographic separation of the methanol eluate of the HP20 resins. The eluate was dried under reduced pressure, dissolved in a minimal volume of methanol and applied to HP20 column chromatography, which was developed with water and an increment of methanol. Both **13** and **14** were eluted in 100% methanol, while **13** was eluted faster than **14**. The early fractions enriched with **13** were applied to ODS-A gel column chromatography, which was developed with water and an increment of methanol. The fractions containing **13** were collected to be applied to silica gel column chromatography, which was developed with n-hexane and an increment of ethylacetate, to afford approximately 50 mg of **13**. The HP20 methanol fractions that were enriched in **14** were processed with silica gel column chromatography to afford approximately 25 mg of **14**.

High resolution mass analysis was conducted in FAB (positive mode) ionization method and this verified the identities of **13** and **14** as the unreduced congener by the detection of 373.1649 and 401.1967 *m/z* signals, respectively, for $[M+H]^+$ ions, where the calculated exact masses are 373.1651 ($C_{21}H_{25}O_6^+$) and 401.1964 ($C_{23}H_{29}O_6^+$), respectively. The main fragmentation ion peaks were found at *m/z* 136, 154, and 274 for both **13** and **14** in a low resolution FAB mass analysis. The specific rotation ($[?]_D$) values of **13** and **14** were +256.2 and +154.7 (*c* 0.1, CH_3OH), respectively. UV-visible absorption spectra of **13** and **14** were indistinguishable, displaying the absorption peaks at 265 and 340 nm (Fig. S8). The pH dependency of the UV-visible absorption spectra is notable for **3** to **6**. Azs **3** and **4** turned red and then purple, displaying a red-shift in the spectra, with the increase of pH [30]. The UV-visible absorption spectra of **13** and **14** also showed a pH dependency and the increase of pH generated an absorption peak at 527 nm (Fig. S9). The yellow color of **13** and **14** turned orange at pH 6.0 and then red at pH 8.0 and 10.0.

The isolated compounds were subjected to nuclear magnetic resonance (NMR) analysis. The collected NMR data were consistent with the proposed structures of **13** and **14** (Table 1). The ^{1}H- and ^{13}C-NMR spectra of **13** appeared closely related to those of **14** and the NMR spectra

Table 1. ^{1}H (400 MHz) and ^{13}C (100 MHz) spectral data ($CDCl_3$) for **13** and **14**.

C No.	δ ^{1}H (ppm) (multi., J_{HH} in Hz)		δ ^{13}C (ppm)		HMBC	
	13	**14**	**13**	**14**	**13**	**14**
1	8.76 (s)	8.77 (s)	153.6	153.4	-	-
3	-	-	159.7	159.4	1, 4, 11	1, 4, 11
4	6.20 (s)	6.18 (s)	109.7	109.7	5, 11	5, 11
4a	-	-	144.3	143.9	1, 4, 5	1, 5
5	5.25 (s)	5.28 (s)	105.1	105.3	4, 10	4, 10
6	-	-	190.5	190.4	10	10
6a	-	-	87.6	87.6	5, 10	5, 10
8	-	-	168.2	168.1	-	-
9	-	-	123.5	123.6	-	-
9a	-	-	165.3	165.1	1, 4, 10	1, 10
9b	-	-	111.2	111.3	1, 4, 5	1, 4, 5
10	1.63 (s)	1.66 (s)	26.2	26.2	-	-
11	2.55 (n.d.)	2.56 (n.d.)	42.6	42.6	4, 12, 13,	4, 13
12	4.17 (m)	4.19 (m)	65.2	65.3	11, 13	11, 13
13	1.29 (d, 6)	1.31 (d, 6)	23.6	23.7	11, 12	11
14	-	-	197.1	197.1	15	15
15	3.11 (ddd, 6, 9, 15), 2.75 (ddd, 6, 9, 15)	3.14 (ddd, 6, 9, 15), 2.75 (ddd, 6, 9, 15)	42.0	42.1	16	16
16	1.55 (n.d.)	1.55 (n.d.)	22.9	23.3	15	15
17	1.26 (n.d.)	1.25 (n.d.)	31.1	28.9	19	15
18	1.25 (n.d.)	1.25 (n.d.)	22.4	29.0	19	n.d.
19	0.82 (t, 7)	1.21 (n.d.)	13.9	31.6	18	20, 21
20		1.25 (n.d.)		22.5		19, 21
21		0.84 (t, 7)		14.0		20

n.d.; not determined

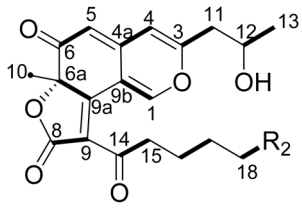

13 (R_2 = -CH_3); **14** (R_2 = -$(CH_2)_2CH_3$)

can be found in Figs. S10–S13. ^{13}C-NMR analysis revealed 21 and 23 carbon signals for **13** and **14**, respectively. When compared to **13**, two additional ^{13}C signals were found at 28.9 and 29.0 ppm for **14**. These additional signals of **14** are assigned for methylene carbons of *C*-19 and *C*-20. The ^{1}H-NMR analysis of **13** showed three olefinic singlet hydrogen signals at 8.76, 6.20, and 5.25 ppm, which are assigned to alkenyl hydrogens at C1, C4, and C5, respectively. These downfield signals, together with the singlet methyl hydrogen (10-*H*) signal at 1.63 ppm, are characteristic of the azaphilone structure. The 1-*H* signal correlates with that of the 5-*H* signal and weakly to that of 4-*H* in the COSY spectrum. HSQC analysis was used to assign *C*-1, *C*-4 and *C*-5 ^{13}C signals at 153.6, 109.7, and 105.1 ppm, respectively. The *C*-4 ^{13}C signal (109.7 ppm) correlates with the 5-*H* signal (5.25 ppm) and the ^{1}H signals (2H; these two proton signals are not resolved in this analysis) at 2.55 ppm. The latter ^{1}H signals are assigned as those of 11-*H* (*C*-11 ^{13}C signal at 42.6 ppm). The 11-*H*- and *C*-11 signals were used to define the ^{1}H and ^{13}C signals for *C*-12 and *C*-13. The chemical shift (4.17 ppm) of the 12-*H* signal (1H) is characteristic of the hydroxymethine hydrogen. The *C*-5 ^{13}C signal (105.1 ppm) correlates to the 4-*H* signal (6.20 ppm) and the 10-*H* signal (1.63 ppm). The *C*-1 signal showed no

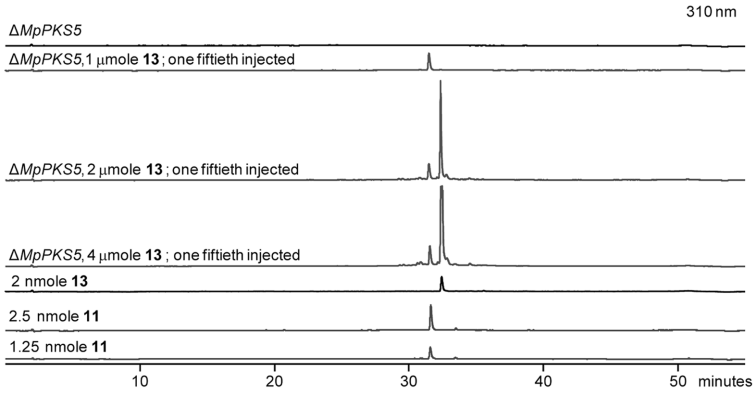

Fig. 4. The *M. purpureus* Δ*MpPKS5* strain converted **13** to **11**.

UV-absorption traces of HPLC analysis, monitored at 330 nm and drawn to the same Y-scale, are shown for the SN extracts of the Δ*MpPKS5* control, the Δ*MpPKS5* with **13** (1, 2, or 4 μmoles; one fiftieth applied to HPLC), authentic samples of **13** (2 nmoles) and **11** (2.5 or 1.25 nmoles). The bioconversion extract from the 5 μl culture was dissolved in 50 μl methanol from which 1 μl was applied to HPLC. The SN was extracted with chloroform.

correlation in HMBC. In the HMBC spectrum of **13**, the 10-*H* singlet methyl hydrogen signal (1.63 ppm) correlates to a carbonyl carbon at 190.5 ppm (*C*-6), a quaternary carbon at 87.8 ppm (*C*-6a), a tertiary carbon at 105.1 ppm (*C*-5) and a quaternary carbon at 165.3 ppm. The last signal is thus assigned to *C*-9a. This *C*-9a ^{13}C signal was also correlated with the 1-*H* signal. The ^{13}C signals at 123.5 and 168.2 ppm are assigned to *C*-9 and *C*-8. These carbons do not correlate to a proton signal. This observation suggests the presence of an unsaturated γ-butyrolactone moiety composed of *C*-6a, *C*-8, *C*-9, and *C*-9a that bears a double bond between *C*-9 and *C*-9a. The NMR spectra of **14** are almost identical to those of **13** with a few exceptions, as mentioned above.

Bioconversion of 13 to 11 in *M. purpureus*

We hypothesized that **13** and **14** are reduced into **11** and **12**, respectively, in MAz biosynthesis (Fig. 1). To verify this idea, biotransformation of **13** was conducted in *M. purpureus* strains. First, the Δ*MpPKS5* strain was used because detecting any pigment was straightforward in this albino strain [16]. When **13** (0.2, 0.4 and 0.8 mM) was added to the Δ*MpPKS5* culture, **11**, in addition to intact **13**, could be found in the SN extract by TLC analysis (Fig. S14). There was no significant change in **11** that was fed to the Δ*MpPKS5* strain. Az **11** was also found in the cell extract when **13** was supplemented, and there was no evidence of **13** in these cell extracts (Fig. S14). This suggests that cell penetration of **13** is limited, but it was quantitatively converted to **11** once it entered the cell. HPLC analysis further supported the conversion of **13** to **11** in the Δ*MpPKS5* strain (Fig. 4). Approximately 0.1 μmole of **11** was found in the SN extract when 1 μmole of **13** was applied. An increase in **13** or a longer incubation failed to enhance the yield of **11** (data not shown). There are four oxidoreductase genes (*mppA*, *mppC*, *mppE*, and *mppG*) in MAz BGC [17, 23, 24]. We tested the four gene inactivation strains of these oxidoreductase genes for the reduction activity converting **13** to **11**. All the strains retained the reduction activity (Figs. S15 and S16), indicating that the reduction of **13** into **11** was not mediated by a catalyst encoded in MAz BGC.

This study provides an example of inducing accumulation of cryptic fungal metabolites by HP20-EF. We demonstrated that HP20-EF is capable of inducing the accumulation of intermediate compounds in MAz biosynthesis from the recombinant *M. purpureus* Δ*mppC* and Δ*mpp7* strains by trapping them in the SN. This method unveiled two novel Az compounds from the Δ*mpp7* strain. HP20-EF could serve as a simple fermentation technique to accumulate intermediate Az metabolites to expand the isolable inventory of Az.

Acknowledgment

This research was supported by the Basic Science Research Program through the National Research Foundation of Korea (NRF) funded by the Ministry of Education (NRF-2016R1D1A1B02009237).

Conflict of Interest

The authors have no financial conflicts of interest to declare.

References

1. Wang TH, Lin TF. 2007. *Monascus* rice products. *Adv. Food Nutr. Res.* **53:** 123-159.
2. Feng Y, Shao Y, Chen F. 2012. *Monascus* pigments. *Appl. Microbiol. Biotechnol.* **96:** 1421-1440.
3. Patakova P. 2013. *Monascus* secondary metabolites: production and biological activity. *J. Ind. Microbiol. Biotechnol.* **40:** 169-181.
4. Gao JM, Yang SX, Qin JC. 2013. Azaphilones: chemistry and biology. *Chem. Rev.* **113:** 4755-4811.
5. Chen W, He Y, Zhou Y, Shao Y, Feng Y, Li M, *et al*. 2015. Edible filamentous fungi from the species *Monascus*: early traditional fermentations, modern molecular biology, and future genomics. *Compr. Rev. Food Sci. Food Saf.* **14:** 555-567.
6. Lee CL, Hung YP, Hsu YW, Pan TM. 2013. Monascin and ankaflavin have more anti-atherosclerosis effect and less side effect involving increasing creatinine phosphokinase activity than monacolin K under the same dosages. *J. Agric. Food Chem.* **61:** 143-150.
7. Hsu WH, Pan TM. 2014. A novel PPARgamma agonist monascin's potential application in diabetes prevention. *Food Funct.* **5:** 1334-1340.
8. Chang YY, Hsu WH, Pan TM. 2015. *Monascus* secondary metabolites monascin and ankaflavin inhibit activation of RBL-2H3 cells. *J. Agric. Food Chem.* **63:** 192-199.
9. Lee CL, Wen JY, Hsu YW, Pan TM. 2013. *Monascus*-fermented yellow pigments monascin and ankaflavin showed antiobesity effect via the suppression of differentiation and lipogenesis in obese rats fed a high-fat diet. *J. Agric. Food Chem.* **61:** 1493-1500.
10. Lin CH, Lin TH, Pan TM. 2017. Alleviation of metabolic syndrome by monascin and ankaflavin: the perspective of *Monascus* functional foods. *Food Funct.* **8:** 2102-2109.
11. Wang YR, Liu SF, Shen YC, Chen CL, Huang CN, Pan TM, *et al.* 2017. A randomized, double-blind clinical study to determine the effect of ANKASCIN 568 plus on blood glucose regulation. *J. Food Drug Anal.* **25:** 409-416.
12. Liu SF, Wang YR, Shen YC, Chen CL, Huang CN, Pan TM, *et al.* 2018. A randomized, double-blind clinical study of the effects of Ankascin 568 plus on blood lipid regulation. *J. Food Drug Anal.* **26:** 393-400.
13. Zheng Y, Xin Y, Shi X, Guo Y. 2010. Cytotoxicity of *Monascus* pigments and their derivatives to human cancer cells. *J. Agric. Food Chem.* **58:** 9523-9528.
14. Zheng Y, Xin Y, Shi X, Guo Y. 2010. Anti-cancer effect of rubropunctatin against human gastric carcinoma cells BGC-823. *Appl. Microbiol. Biotechnol.* **88:** 1169-1177.
15. Zheng Y, Zhang Y, Chen D, Chen H, Lin L, Zheng C, *et al.* 2016. *Monascus* pigment rubropunctatin: a potential dual agent for cancer chemotherapy and phototherapy. *J. Agric. Food Chem.* **64:** 2541-2548.
16. Balakrishnan B, Karki S, Chiu SH, Kim HJ, Suh JW, Nam B, *et al.* 2013. Genetic localization and in vivo characterization of a *Monascus* azaphilone pigment biosynthetic gene cluster. *Appl. Microbiol. Biotechnol.* **97:** 6337-6345.
17. Bijinu B, Suh JW, Park SH, Kwon HJ. 2014. Delineating *Monascus* azaphilone pigment biosynthesis: oxidoreductive modifications determine the ring cyclization pattern in azaphilone biosynthesis. *RSC Adv.* **4:** 59405-59408.
18. Balakrishnan B, Chandran R, Park SH, Kwon HJ. 2015. A new protein factor in the product formation of non-reducing fungal polyketide synthase with a *C*-terminus reductive domain. *J. Microbiol. Biotechnol.* **25:** 1648-1652.
19. Zabala AO, Xu W, Chooi YH, Tang Y. 2012. Characterization of a silent azaphilone gene cluster from *Aspergillus niger* ATCC 1015 reveals a hydroxylation-mediated pyran-ring formation. *Chem. Biol.* **19:** 1049-1059.
20. Chen W, Chen R, Liu Q, He Y, He K, Ding X, *et al*. 2017. Orange, red, yellow: biosynthesis of azaphilone pigments in *Monascus* fungi. *Chem. Sci.* **8:** 4917-4925.
21. Balakrishnan B, Kim HJ, Suh JW, Chen CC, Liu KH, Park SH, *et al.* 2014. *Monascus* azaphilone pigment biosynthesis employs a dedicated fatty acid synthase for short chain fatty acyl moieties. *Kor. Soc. Appl. Biol. Chem*. **57:** 191-196.
22. Balakrishnan B, Chen CC, Pan TM, Kwon HJ. 2014. Mpp7 controls regioselective Knoevenagel condensation during the biosynthesis of *Monascus* azaphilone pigments. *Tetrahedron Lett.* **55:** 1640-1643.
23. Balakrishnan B, Park SH, Kwon HJ. 2017. A reductase gene *mppE* controls yellow component production in azaphilone polyketide pathway of *Monascus*. *Biotechnol. Lett.* **39:** 163-169.
24. Balakrishnan B, Park SH, Kwon HJ. 2017. Inactivation of the oxidase gene *mppG* results in the selective loss of orange azaphilone pigments in *Monascus purpureus*. *Appl. Biol. Chem.* **60:** 437-446.
25. Hu Z, Zhang X, Wu Z, Qi H, Wang Z. 2012. Perstraction of intracellular pigments by submerged cultivation of *Monascus* in nonionic surfactant micelle aqueous solution. *Appl. Microbiol. Biotechnol.* **94:** 81-89.
26. Kang B, Zhang X, Wu Z, Qi H, Wang Z. 2013. Effect of pH and nonionic surfactant on profile of intracellular and extracellular *Monascus* pigments. *Process Biochem.* **48:** 759-767.
27. Xiong X, Zhang X, Wu Z, Wang Z. 2015. Accumulation of yellow *Monascus* pigments by extractive fermentation in nonionic surfactant micelle aqueous solution. *Appl. Microbiol. Biotechnol.* **99:** 1173-1180.
28. Shi K, Tang R, Huang T, Wang L, Wu Z. 2017. Pigment fingerprint profile during extractive fermentation with *Monascus anka* GIM 3.592. *BMC Biotechnol.* **17:** 46.
29. Lim YJ, Lee DW, Park SH, Kwon HJ. 2018. Extractive fermentation of *Monascus purpureus* promotes the production of oxidized congeners of the pigment azaphilone. *J. Appl. Biol. Chem.* **61:** 327-334.
30. Shi K, Chen G, Pistolozzi M, Xia F, Wu Z. 2016. Improved analysis of *Monascus* pigments based on their pH-sensitive Uv-Vis absorption and reactivity properties. *Food Addit. Contam. Part A Chem. Anal. Control Expo. Risk Assess* **33:** 1396-1401.